Interface-Engineered Bistable [2]Rotaxane-Graphene Hybrids with Logic Capabilities

Chuancheng Jia, Hao Li, Jiaolong Jiang, Jindong Wang, Hongliang Chen, Dennis Cao, J. Fraser Stoddart, and Xuefeng Guo**

In recent years, interest in the marriage of graphenes as sensing elements integrated with other materials has grown, creating hybrid optoelectronic devices for potential applications in areas ranging from integrated circuits and energy conversion to catalysis and chemobiological sensors.[1–5] Their high chemical stability,[6] availability through bottom-up growth,[7] and relative ease of micro/nanofabrication,[8,9] position graphenes as attractive platforms for building new types of sensors and optoelectronic devices.[10] Although previous reports have already demonstrated the remarkable performance of nanoscale graphene-based hybrid devices, issues associated with working mechanisms,[11–13] detection sensitivity,[4,14] and optimised device layouts are still under intense investigation. These challenges illustrate that, at the microscopic level, the fundamental understanding of these promising devices is far from well-established. This incompleteness largely results from the ambiguity associated with interfaces built from graphene derivatives such as graphene oxide or reduced graphene oxide,[2,15] and the lack of efficacious strategies for graphene modification and device operation which preserve the pristine structure and properties of graphene.[6,16] In this investigation, we demonstrate the rational design of a hybrid redox-bistable [2]rotaxane-graphene photoswitch whose mirror-image photoswitching and non-volatile memory effects in a single graphene sheet allow us to establish a mechanistic understanding of the charge generation/trapping processes at the [2]rotaxane-graphene interface by using high-quality graphenes as local probes in combination with photoirradiation (**Figure 1**a,b).

C. Jia,[+] J. Jiang, J. Wang, H. Chen, Prof. X. Guo
Center for NanoChemistry, Beijing National Laboratory for Molecular Sciences
State Key Laboratory for Structural Chemistry of Unstable and Stable Species
College of Chemistry and Molecular Engineering
Peking University
Beijing, 100871, P. R. China
E-mail: guoxf@pku.edu.cn
Dr. H. Li,[+] D. Cao, Prof. J. F. Stoddart
Department of Chemistry
Northwestern University
2145 Sheridan Road, Evanston, IL 60208, USA
E-mail: stoddart@northwestern.edu
Prof. Dr. X. Guo
Department of Materials Science and Engineering
College of Engineering
Peking University
Beijing, 100871, P. R. China
[+]These authors contributed equally to the work.

DOI: 10.1002/adma.201302393

The graphene-based hybrid device incorporates a bistable [2]rotaxane $\mathbf{R}^{8+}$ – rotaxanes are a class of mechanically interlocked molecules (MIMs) which have been employed[17] in a variety of potential applications in molecular nanotechnology – whose ring component is known[18] to undergo discrete translational motion along the dumbbell component upon external stimulus. In this photoswitchable [2]rotaxane, the cyclobis(paraquat-*p*-phenylene) ($CBPQT^{4+}$) ring encircles a dumbbell which consists of: i) a photocatalytic ruthenium(II)-tris(2,2′-bipyridine) ($[Ru(bpy)_3]^{2+}$) stopper, ii) a π-electron rich 1,5-dioxynaphthalene (DNP) recognition site, iii) a 4,4′-bipyridinium ($BIPY^{2+}$) unit, and iv) a hydroxyl function for attachment to the graphene surface (Figure 1c).

The functioning molecular component of the hybrid device originates from a monolayer of bistable rotaxanes $\mathbf{R}^{8+}$ in which light-activated reduction of the MIM leads to: i) the formation of a positively-charged trisradical complex ($BIPY^{\bullet+}\subset CBPQT^{2(\bullet+)}$) that brings the ring closer to the graphene surface, thus creating a different built-in electrical field at the MIM-graphene interface[19] which changes the conductance of the graphene sheet through geometrically and electrostatically-induced capacitive coupling[20] as well as ii) a change in the electronic structure at the interface which alters the carrier density and corresponding channel conductance of graphene. The synergic effects of electrostatic gating and changes in electronic structure highlight the important roles of both the light-stimulated translational motion of the rings in the bistable [2]rotaxanes and the gate-tunable ambipolar transport property of graphene in the performance of the logic-controllable hybrid device.

The device (Figure 1a) consists of a single-layer graphene sheet used as the conductive channel placed on top of a doped silicon wafer with 300 nm of thermally grown SiO_2 on the surface and a monolayer of $\mathbf{R}^{8+}$ as the light sensitiser that is noncovalently assembled on the graphene surface by a nondestructive step-wise procedure (Figure 1b). The [2]rotaxane $\mathbf{R}\bullet 8PF_6$ was synthesized by taking advantage of a template-directed strategy and was fully characterized by NMR spectroscopy and mass spectrometry (see Supporting Information). In order to demonstrate the efficiency of the design, high-quality CVD-grown graphene-based transistors with a channel length of ≈5 μm were built by using a method we developed[9] previously for the fabrication of single-molecule devices and real-time measurements (see the Supporting Information). This method enables the mass-production of high-density graphene transistor arrays in high yield (≈98%) (**Figure 2**a,b). In the Raman spectrum of the graphene utilized (Figure 2c), a single symmetric 2D peak (≈2650 cm^{-1}) with narrow peak width, a small G/2D ratio, and a negligible D peak were observed, indicating that the graphene is single-layered and of high quality.[21] All the devices

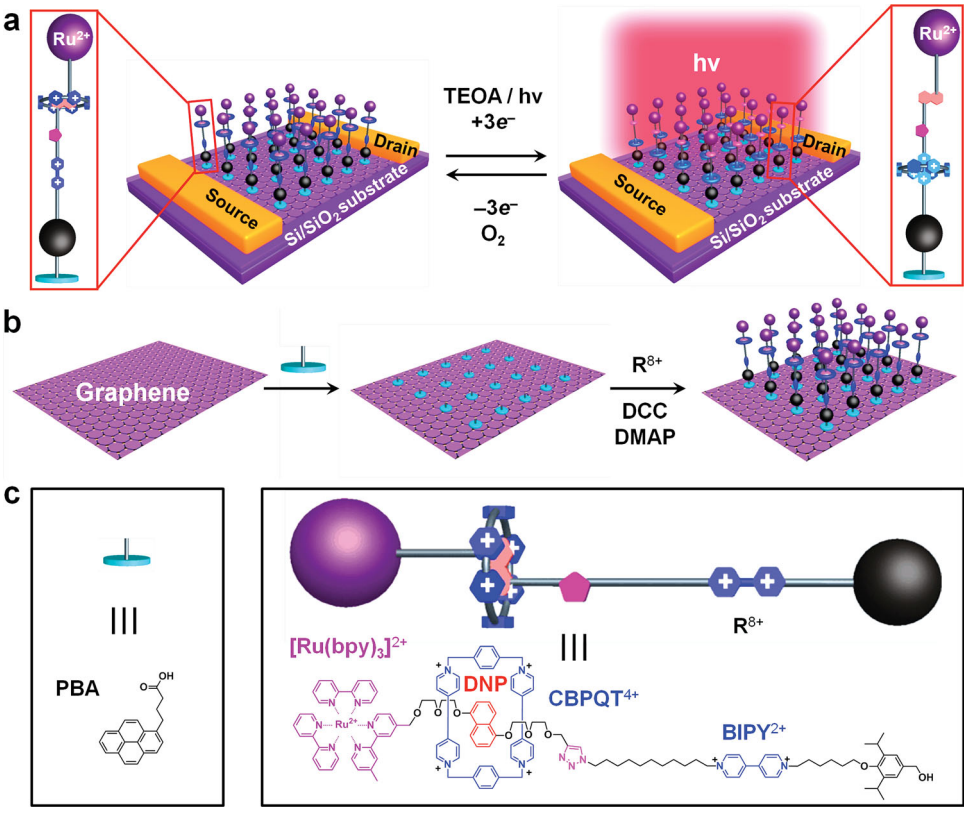

Figure 1. a) Schematic representation of graphene transistors decorated with light-activated switchable [2]rotaxanes in the presence of triethanolamine (TEOA) as a sacrificial electron donor. b) The two-step strategy employed in the assembly of the bistable [2]rotaxane molecules onto a graphene surface without altering the structure and properties of graphene covalently. c) The structural formulas and graphical representations of the 1-pyrenebutanoic acid (PBA) used to link the bistable [2]rotaxane molecules noncovalently to the surface of the graphene.

exhibit p-type electric field effects with little gate-dependence before the molecular assembly process because the neutrality point (V_{Dirac}) is shifted to more positive values, most likely on account of chemical doping and/or charge transfer induced by the etching agents and polymer resists used (Figure S4, Supporting Information).[7,9]

After the initial characterisation, the graphene devices were immersed into a MeCN solution of 1-pyrenebutanoic acid (PBA) which binds noncovalently with the graphene surface by means of π–π stacking interactions.[22] An absorption band centered at ≈360 nm was observed in the solid-state UV–Vis absorption spectrum of the resultant graphene (Figure 2d), confirming that the PBA molecules are adsorbed on the graphene's surface (Figure S5, Supporting Information). The bistable [2]rotaxanes were then tethered to the modified graphene surface by esterification of their hydroxyl terminal groups with the carboxylic acid groups of the surface-bound PBA molecules in high yield (≈98%). The assemblies are able to survive rinsing and even soaking with prolonged sonication in common solvents, such as MeCN and CH_2Cl_2, to remove any unreacted rotaxane molecules. A maximum absorption band centered at ≈470 nm, which corresponds to the $Ru(bpy)_3^{2+}$ dicationic unit in the bistable [2]rotaxane (Figure S5, Supporting Information),[18] was observed in the solid-state UV–Vis absorption spectrum of the device. (Figure 2d). High-resolution X-ray photoelectron spectroscopy (XPS) of the bistable [2]rotaxane-graphene hybrids also revealed the emergence of the N1s peak (Figure 2e and Figure S6, Supporting Information) which is not present in the PBA-decorated graphene. These observations, in combination with Fourier transform infrared (FTIR) and Raman spectroscopy (Figure S7, Supporting Information), prove that the bistable [2]rotaxane has been successfully grafted onto the graphene surface. After the molecular deposition, the devices showed a slight conductance decrease (Figure S4, Supporting Information), most likely because of n-type doping created by bistable [2]rotaxanes that are in intimate contact with the graphene surface.

In order to expose the bistable [2]rotaxane-graphene hybrid device to triethanolamine (TEOA) under operating conditions, we integrated a microfluidic setup (Figure 2a,b) into the device system designed to operate under strictly oxygen-free conditions (Figure S8, Supporting Information). The microfluidic channels, which are ≈100 μm tall and ≈250 μm wide, were fabricated by means of soft-lithography and replica molding techniques as detailed in the Supporting Information.[23] The microfluidic channels enabled us to monitor the activity of the bistable rotaxane molecules in real time by using graphene as reporters in combination with photoillumination (30 μW/cm^2,

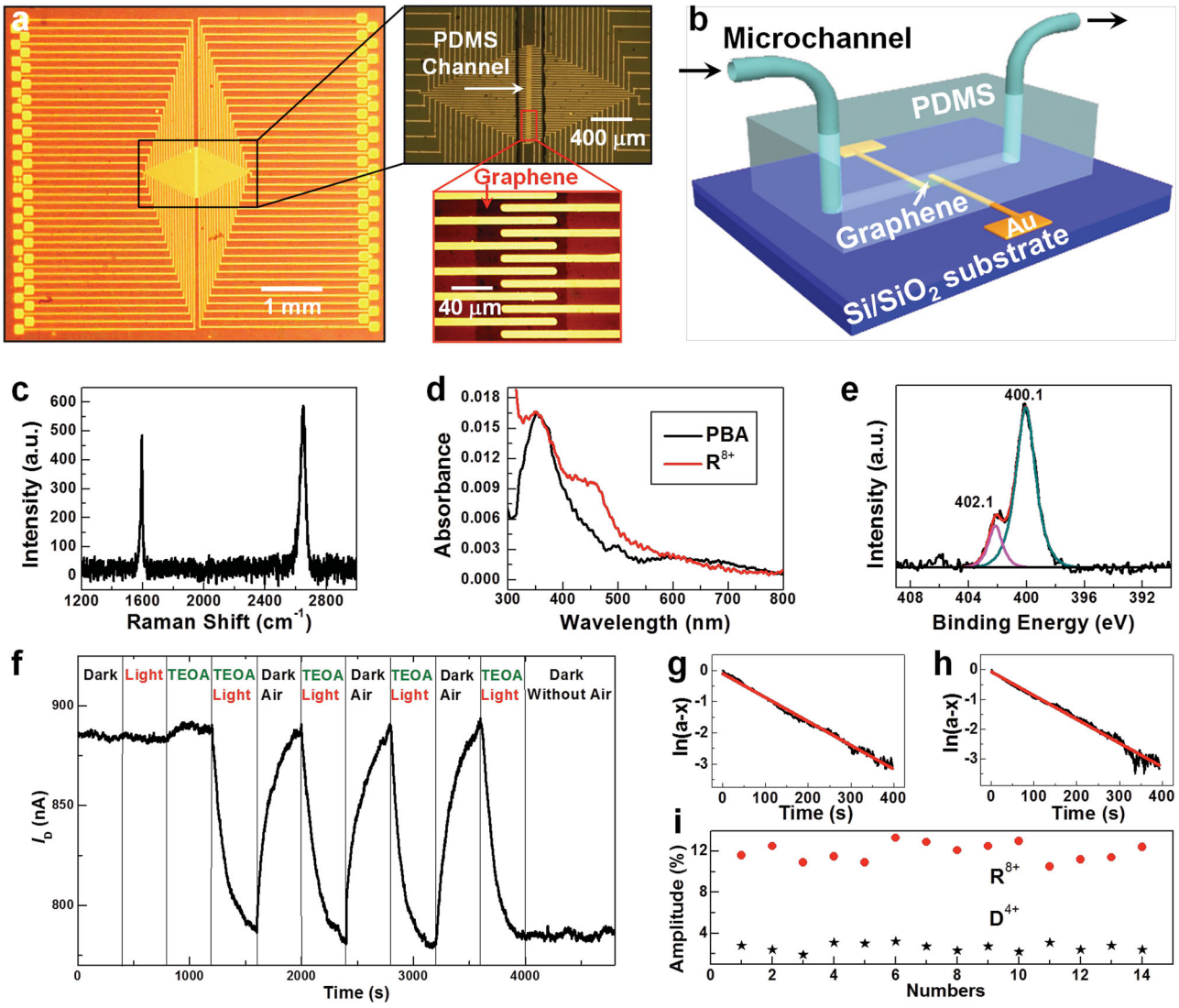

Figure 2. a) An optical image of a high-density graphene transistor array. The insets show the enlarged optical images of the central parts with microfluidics as marked, respectively. b) Schematic representation of the experimental setup with the microfluidic system. c) The Raman spectrum of graphene employed in this research. d) UV–Vis absorption spectra of PBA- and [2]rotaxane-decorated CVD-grown graphenes on quartz substrates, respectively. In order to clearly show the comparison, the absorbance of graphene has been removed in both cases. e) High-resolution XPS spectrum of the N (1s) region for [2]rotaxane-decorated graphenes. f) The I_D–t plot for a [2]rotaxane-decorated CVD-grown graphene under different conditions: initial injection of the MeCN solution in the dark, only light irradiation, only TEOA addition, both light and TEOA, dark with air and dark without air. V_D = 1 mV. V_G = 0 V. g,h) Kinetic simulations of the intramolecular switching within the bistable [2]rotaxanes under light illumination in the presence of TEOA (g), followed by keeping in the dark with air exposure (h). i) The statistical comparison of the change ratios in I_D of graphenes after bistable [2]rotaxane (red circles) and dumbbell (black stars) modifications, respectively, under light illumination in the presence of TEOA.

>450 nm). In order to eliminate the possibility of electrode surface and/or Schottky barrier modifications, we passivated the metal electrodes with a 50 nm-thick silicon oxide layer as a protective layer before the photoresist lift-off and molecular grafting. Unlike previously reported graphene-based photosensors in which photoinduced current changes occur mostly at the contact interface between the graphene and the electrodes[24] or in the vicinity of p-n junctions,[25,26] the bistable [2]rotaxane-graphene hybrid system is photoresponsive over a large area (Figure 1a), a feature of paramount importance in many sensing applications.[3,27]

We have found that large and reversible changes in source-drain current (I_D) occur in these bistable [2]rotaxane-decorated graphene devices upon proper external stimuli (Figure 2f). After completely stabilizing the devices by first flowing deoxygenated MeCN solution through the microfluidic channel, the simultaneous application of both light and TEOA leads to an obvious decrease (≈12%) in the I_D of the graphene. Subsequent exposure of the devices to oxygen in the dark almost reinstates the initial I_D, thus accomplishing a full switching cycle. Control experiments using graphenes decorated only by PBA did not show any obvious current changes when exposed to the

same conditions (Figure S9, Supporting Information), thus ruling out the possibility that the conductance changes of the bistable [2]rotaxane-decorated graphene devices result from any intrinsic light-triggered processes in either the graphene sheets or the PBA molecules. These results suggest that the light-stimulated translational movement of the rings in the $\mathbf{R}^{8+}$ molecules plays a key role in the switching properties of the devices.

When the operations are alternated sequentially in the presence of TEOA, the devices display excellent reversibility as demonstrated in Figure 2f (3 representative cycles out of more than 20 cycles). Additionally, when the devices are kept in the dark in the absence of oxygen after light and TEOA treatments, the low conductance state of the devices remains constant for 24 hours (some data shown in Figure 2f). The non-volatility of the low conductance state in the bistable [2]rotaxane-graphene hybrid and the stable I_D of the graphene (Figure 2f) lies in stark contrast to the decay of photogenerated conductance in previously reported graphene-based photodetectors when the devices are left in the dark.[13,24,25] This observation is not surprising because both of these two inputs are required to trigger the translational motion of the ring in the bistable [2]rotaxane.[18] In order to understand the kinetics of the ring's motion, we have analysed the conductance data extracted from Figure 2f as a function of time (Figure 2g,h). Both the forward and backward reactions can be fitted to linear first-order equations of the type $\ln(a - x) = \ln(I_t - I_{400s})/(I_{0s} - I_{400s})$, with calculated rate constants of $\approx 7.65 \times 10^{-3}$ s^{-1} and $\approx 7.99 \times 10^{-3}$ s^{-1}, respectively.

After detailing the specifics of the devices, we turned our attention to describing the physical mechanism underlying the observed photoswitching behavior. In order to compare the electronic structures at the bistable [2]rotaxane-graphene interface before and after light illumination, we have investigated the electrochemical characteristics of $\mathbf{R}^{8+}$. On the basis of cyclic voltammetric (CV) data (Figure S10, Supporting Information), the lowest unoccupied molecular orbital (LUMO) energy levels of the oxidized bistable [2]rotaxane and the reduced trisradical [2]rotaxane were estimated to be –4.09 and –3.68 eV, respectively, versus the vacuum level for the calculation details (See the Supporting Information). The highest occupied molecular orbital (HOMO) energy levels were found to be –6.81 and –6.00 eV, respectively, according to the energy gaps (≈2.72 eV for oxidized bistable [2]rotaxanes and ≈2.32 eV for reduced trisradical [2]rotaxanes) extracted from UV–Vis absorption spectra (Figure S11, Supporting Information). These calculations reveal that the HOMO of the reduced trisradical [2]rotaxane is close to the Fermi level (≈4.5–4.8 eV) of graphene[28] (**Figure 3**), thus facilitating the electronic communication between the reduced [2]rotaxane molecules and graphene which leads to quenching of the p-type carriers and a decrease in the conductance of the hole-dominated graphene. This quenching effect is further enhanced by the formation of the trisradical triscationic complex ($BIPY^{\bullet+}\subset CBPQT^{2(\bullet+)}$) close to the graphene surface, which

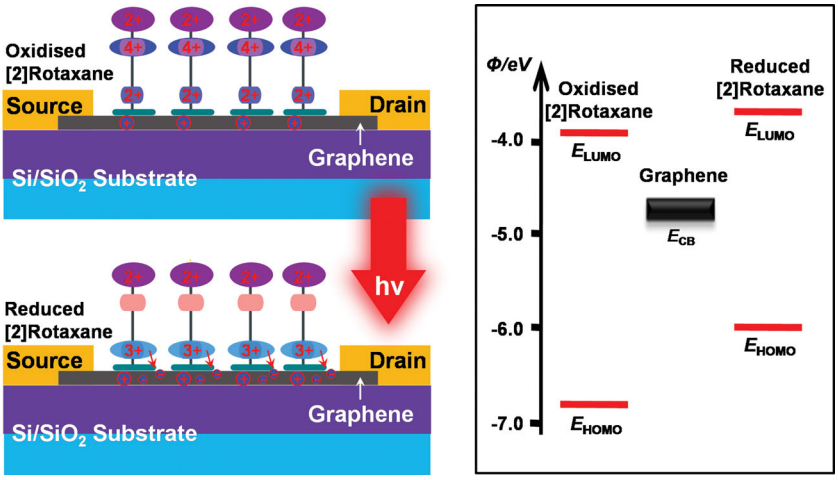

Figure 3. Synergistic photoswitching mechanisms operative in the bistable [2]rotaxane-decorated graphene and energy-level diagram of the bistable [2]rotaxane/graphene interface.

is more positively-charged than the dicationic $BIPY^{2+}$ unit in the fully oxidized state of the [2]rotaxane. In the ground state, the $CBPQT^{4+}$ ring encircles the DNP unit and thereby resides in a position distant from the graphene surface.[29] When the ring is reduced and located closer to the graphene surface, a built-in field is formed at the reduced [2]rotaxane-graphene interface which behaves as a positive top gate that induces negative carriers in the conductive channel through electrostatic gating, thus leading to an increase in the graphene resistance (Figure 3). The non-volatile stability of the low conductance state of the reduced [2]rotaxane-graphene hybrid can be ascribed to the stability of the $BIPY^{\bullet+}\subset CBPQT^{2(\bullet+)}$ complex under oxygen-free conditions, regardless of the presence or absence of light.

In order to prove the importance of the translational movement of the ring component in the bistable [2]rotaxane, we synthesized the photoswitchable non-interlocked control dumbbell $\mathbf{D}\bullet 4PF_6$ (Figure S12, Supporting Information). Graphene was functionalized with $\mathbf{D}\bullet 4PF_6$ following the same procedure described in Figure 1b for $\mathbf{R}\bullet 8PF_6$. The $BIPY^{(\bullet+)}$ radical cation generated by photoillumination of the dumbbell-graphene hybrid device has a stronger electronic coupling with the graphene than does $BIPY^{2+}$ because its HOMO level is closer to the Fermi level of graphene (Figure S13, Supporting Information), thus leading to a reproducible conductance decrease of the devices by a chemical n-doping mechanism (Figure S13b, Supporting Information). The less positively-charged nature of $BIPY^{(\bullet+)}$ increases the positive carrier density in the p-type semiconductor (and thus the device conductance) (Figure S13c, Supporting Information). The combination of these two effects effectively cancel each other out, resulting in a conductance decrease of ≈2.7% (the average value of 2.65% with a standard deviation of 0.39%), which is considerably lower than those observed in the bistable [2]rotaxane-graphene systems (≈12%, the average value of 11.9% with a standard deviation of 0.88%) (Figure 2i).

On the basis of this mechanistic understanding, it can be rationally inferred that the synergistic effects should lead to both a hole-current increase and an electron-current decrease in the same device when an ambipolar material is used. To prove this prediction, a peeling-off approach to obtain pris-

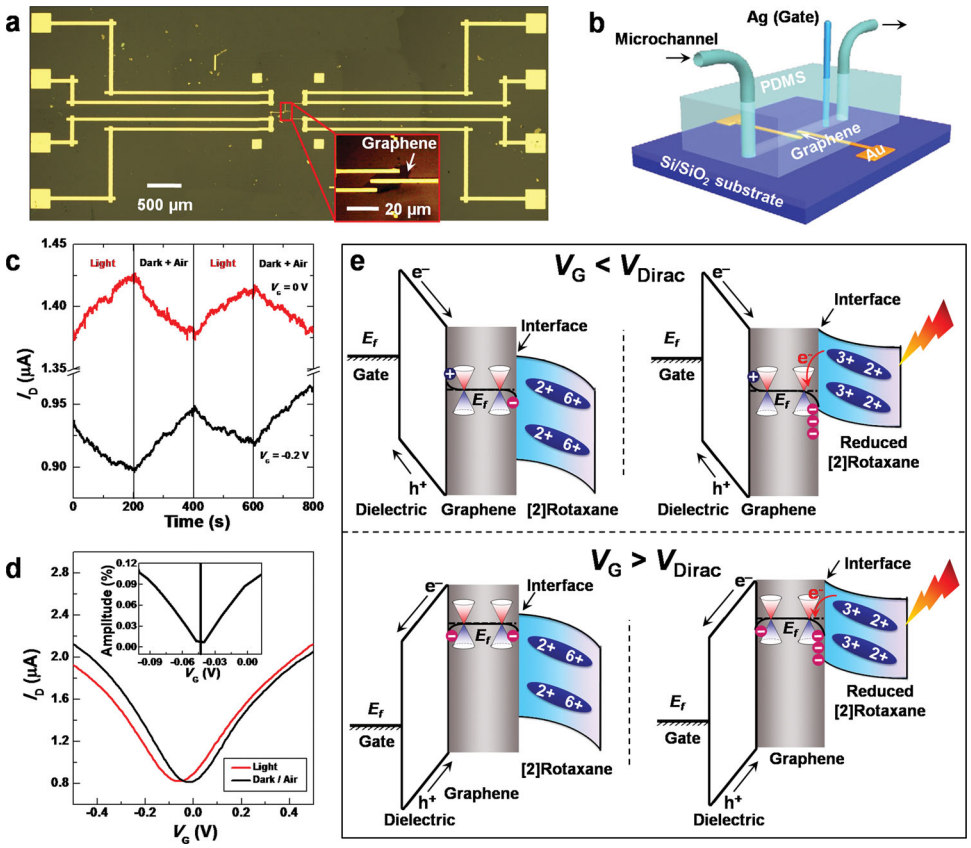

Figure 4. a) An optical image of a device using pristine graphene formed by a peeling-off technique. Inset shows the enlarged optical image of the central part as indicated. b) Schematic representation of the experimental setup which integrates a solution gate through an Ag wire as the reference electrode into the microfluidic system. c) I_D–time plots for the bistable [2]rotaxane-decorated pristine graphene under alternate treatments of light and oxygen in the dark at the different gate biases (top: V_G = 0 V; bottom: V_G = –0.20 V). V_D = 1 mV. The experiments were carried out in a MeCN solution containing 5 mM TEOA and 100 μM tetraethylammonium perchlorate ($TEAClO_4$). d) The gate-dependence of the photoswitching effects in bistable [2]rotaxane-decorated pristine graphenes. V_D = 1 mV. Inset shows the change ratios of I_D as a function of the gate bias, clearly demonstrating a solution-gate-tunable symmetric photoswitching effect. e) Possible models for the band-bending diagrams and charge distribution before (left) and after light illumination (right) in both p-type (top) and n-type (bottom) channels.

tine ambipolar single-layer graphenes[30] that show both electron and hole transport properties was used. After fabricating graphene-based transistors with a channel length of ≈3 μm by the combination of electron-beam lithography and photolithography (**Figure 4**a),[8,9] we have followed the procedure illustrated in Figure 1b to build the bistable [2]rotaxane-decorated graphene devices. A solution gate was introduced into the device system to control the two types of carriers (Figure 4b). This design allows the achievement of stable measurements with high sensitivity at low working voltages.[11,31] The characteristics of the ambipolar devices upon stimuli in presence of TEOA have been recorded (Figure 4c,d). A significant hole current decrease is observed under visible light irradiation when V_G is held at –0.20 V, and the photoswitching process is reversible (Figure 4c) when the light is switched on and off. Remarkably, when V_G is held at 0 V, we observe a large reversible current increase in the same device under the same irradiation conditions. We have extracted the change ratios of I_D as a function of the gate bias from the bias dependence of the photoswitching effect (Figure 4d inset), which clearly reveals a solution-gate-tunable symmetric photoswitching effect.

The observations we have made from the aforementioned experiments allow us to propose a mechanism of photoswitching in the devices. Photon absorption by $[Ru(bpy)_3]^{2+}$ induces the reduction of the $BIPY^{2+}$ units, which motivates translocation of the ring along the dumbbell of the bistable [2]rotaxane to reside closer to the MIM-graphene interface. This relative geometry leads to band bending at the interface (Figure 4e), which favors electron transfer from the [2]rotaxane molecules to the graphene, and also leads to the formation of a local built-in electric field, which behaves as a positive top gate and generates negative carriers in the conductive channel (Figure 4e). This sequence of events may explain the obvious shift of the Dirac point (V_{Dirac}) from –0.02 to –0.06 V (Figure 4d). When $V_G < V_{Dirac}$, graphene is hole-dominated and both light-induced effects consistently cause the increase in resistance or current quenching through chemical n-doping and/or capacitive coupling. When $V_G > V_{Dirac}$, graphene is electron-dominated and light illumination leads to the decrease in resistance. So long as the bistable [2]rotaxane molecules remain reduced, both effects persist, resulting in the non-volatile memory effect.

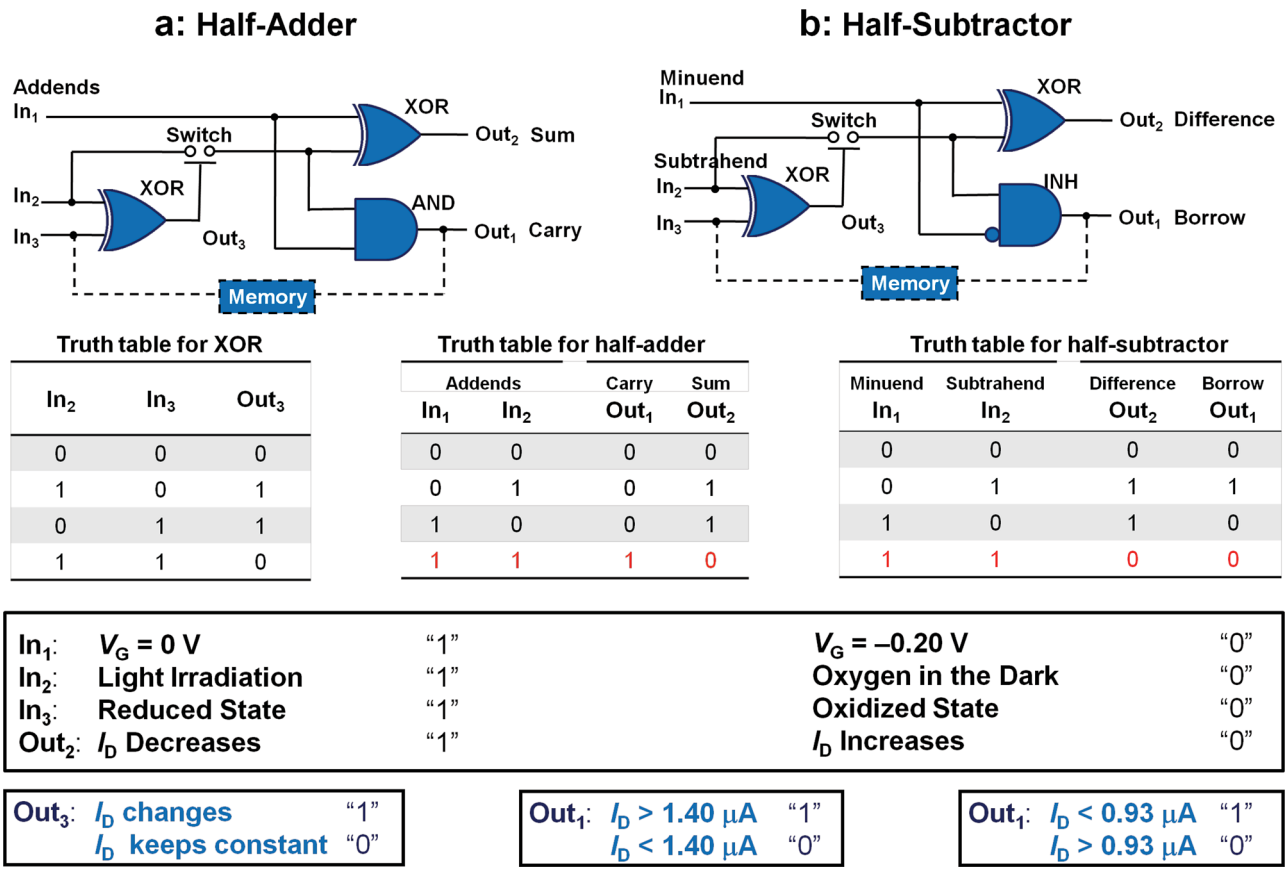

Figure 5. a) Schematic of a half-adder logic circuit and corresponding truth table. b) Schematic of a half-subtractor logic circuit and corresponding truth table. The dash-line parts show that in both cases, further integration of sequential logic into the systems leads to combinational logic computation circuits with a memory effect and resettability.

The photoresponsive behavior of the bistable [2]rotaxane-decorated graphene devices shown in Figure 4c can be endowed with binary logic.[32–34] A combinational logic circuit with memory has been constructed by selecting visible light and oxygen as In_1 and In_2, respectively, with $In_1 = 1$ when the light is on and $In_1 = 0$ when the light is off, while $In_2 = 1$ when oxygen is absent and $In_2 = 0$ when oxygen is present. We chose the I_D of the final states of the [2]rotaxane as the output signal (Out): Out = 1 when $I_D > 1.40$ μA or $I_D < 0.93$ μA (the reduced state); Out = 0 when 0.93 μA < I_D < 1.40 μA (the oxidized state). The output depends, not only on the present input signals, but also on the past history of the input signals (Figure S15, Supporting Information), demonstrating a sequential logic circuit with a memory effect.

A half adder with a basic addition function has been fabricated by choosing the external operations in a rational manner. We chose the gate voltage as the first input signal (V_G, In_1): $In_1 = 1$ when $V_G = 0$ V and $In_1 = 0$ when $V_G = –0.20$ V, and the second input signal (In_2) as follows: $In_2 = 1$ when the light is on and $In_2 = 0$ when oxygen is introduced in the dark. The final drain current (I_D) can be considered as one of the output signals (Out_1): $Out_1 = 1$ when $I_D > 1.40$ μA and $Out_1 = 0$ when $I_D < 1.40$ μA. The direction of current changes can be employed as another output signal (Out_2): $Out_2 = 1$ when I_D decreases and $Out_2 = 0$ when I_D increases. In order to avoid a situation in which I_D remains constant and set the initial states of the bistable [2]rotaxane molecules, we have integrated a switch into the logic circuit by additionally introducing a third input signal (In_3) and third output signal (Out_3) as follows: $In_3 = 1$ when the bistable [2]rotaxane molecules reside in their fully reduced state and $In_3 = 0$ when the molecules are in their fully oxidized state, while $Out_3 = 1$ when I_D changes and $Out_3 = 0$ when I_D remains constant. On the basis of the experimental observations recorded in Figure 4c, when only either of In_2 and In_3 is 1, and the current changes ($Out_3 = 1$), while in other cases, $Out_3 = 0$. Correspondingly, Out_3 in response to the operations of In_2 and In_3 can be interpreted as an XOR logic gate (**Figure 5**a). By using this XOR logic gate to switch on In_2 ($Out_3 = 1$), we are able to fabricate different logic gates (such as AND and XOR) through logic operations of In_1 and In_2. If we employ the final I_D as the output signal (Out_1), then only when $In_1 = 1$ and $In_2 = 1$ (the oxidized state), will $Out_1 = 1$. Otherwise, $Out_1 = 0$, comprising an AND logic gate (Figure S16a, Supporting Information). If we employ the direction of current change as the output signal (Out_2), we find that, when only one input signal (In_1 or In_2) is 1, the current decreases ($Out_2 = 1$), while in other cases, $Out_2 = 0$, thus forming another XOR logic gate. Both AND and XOR logic gates share the same input signals and can be operated in parallel. By combining them together, we realize a basic computation in the form of a half adder that uses

AND as the Carry and XOR as the Sum, respectively. The truth table for the combinational logic half adder is summarized in Figure 5a, demonstrating the binary addition 1 + 1 = 2. In another example, we redefined Out_1 as follows: $Out_1 = 1$ when $I_D < 0.93$ μA and $Out_1 = 0$ when $I_D > 0.93$ μA. As summarized in Figure S16b in the Supporting Information, only in the case of $In_1 = 0$ and $In_2 = 1$, does $Out_1 = 1$, otherwise, $Out_1 = 0$. This situation corresponds to an INH logic gate. Importantly, by interconnecting XOR as the Difference and INH as the Borrow, we were able to mimic the basic subtraction function of a half subtractor (Figure 5b).

A fundamental mechanistic understanding of charge generation/quenching processes underlying the redox-bistable [2]rotaxane-graphene interface has been established by using high-quality graphenes as a tool in combination with photoexcitation. By integrating a nondestructive bottom-up assembly technique with sensitive graphene-based transistors, we have developed a multifunctional optoelectronic device that displays symmetric mirror-image photoswitching with a non-volatile memory effect in a single device. This effect originates from the rational control of the synergistic interfacial effects of chemical n-doping and electrostatic gating, which are induced by light-stimulated reduction-motivated translational motions of the rings in the bistable [2]rotaxanes. These changes in device properties enable the implementation of basic logic computations that are capable of being naturally integrated into current circuit technologies. From a general perspective, the concept of interface engineering demonstrated in this investigation provides new insights into designing interfaces that reveal the intrinsic mechanisms of interface phenomena. They can be employed to elucidate the interplay among parameters that control charge generation, charge transfer, charge recombination, and the final properties of optoelectronic devices. This work sets the stage for a promising universal platform of forming graphene-based hybrids in combination with other materials to create optoelectronic devices with novel functionalities for integrated information technologies and energy conversion applications.

Supporting Information

Supporting Information is available from the Wiley Online Library or from the author.

Acknowledgements

The authors acknowledge primary financial support from MOST (2012CB921404), NSFC (21225311, 51121091, and 2112016), and the 111 Project (B08001). D.C. acknowledges the National Science Foundation (NSF) for a Graduate Research Fellowship as well as support from a Ryan Fellowship sponsored by the Northwestern University International Institute for Nanotechnology.

Received: May 26, 2013
Revised: July 15, 2013
Published online: September 9, 2013

[1] K. S. Novoselov, V. I. Fal'ko, L. Colombo, P. R. Gellert, M. G. Schwab, K. Kim, *Nature* **2012**, *490*, 192.
[2] X. Huang, X. Y. Qi, F. Boey, H. Zhang, *Chem. Soc. Rev.* **2012**, *41*, 666.
[3] W. R. Yang, K. R. Ratinac, S. P. Ringer, P. Thordarson, J. J. Gooding, F. Braet, *Angew. Chem. Int. Ed.* **2010**, *49*, 2114.
[4] F. Schedin, A. K. Geim, S. V. Morozov, E. W. Hill, P. Blake, M. I. Katsnelson, K. S. Novoselov, *Nat. Mater.* **2007**, *6*, 652.
[5] K. P. Loh, Q. L. Bao, P. K. Ang, J. X. Yang, *J. Mater. Chem.* **2010**, *20*, 2277.
[6] D. C. Elias, R. R. Nair, T. M. G. Mohiuddin, S. V. Morozov, P. Blake, M. P. Halsall, A. C. Ferrari, D. W. Boukhvalov, M. I. Katsnelson, A. K. Geim, K. S. Novoselov, *Science* **2009**, *323*, 610.
[7] X. Li, W. Cai, J. An, S. Kim, J. Nah, D. Yang, R. Piner, A. Velamakanni, I. Jung, E. Tutuc, S. K. Banerjee, L. Colombo, R. S. Ruoff, *Science* **2009**, *324*, 1312.
[8] Y. Cao, Z. M. Wei, S. Liu, L. Gan, X. F. Guo, W. Xu, M. L. Steigerwald, Z. F. Liu, D. B. Zhu, *Angew. Chem. Int. Ed.* **2010**, *49*, 6319.
[9] Y. Cao, S. H. Dong, S. Liu, L. He, L. Gan, X. M. Yu, M. L. Steigerwald, X. S. Wu, Z. F. Liu, X. F. Guo, *Angew. Chem. Int. Ed.* **2012**, *51*, 12228.
[10] a) F. S. F. Schwierz, *Nat. Nanotechnol.* **2010**, *5*, 487; b) A. K. Geim, *Science* **2009**, *324*, 1530; c) C. N. R. Rao, A. K. Sood, K. S. Subrahmanyam, A. Govindaraj, *Angew. Chem. Int. Ed.* **2009**, *48*, 7752; d) D. C. Wei, Y. Q. Liu, *Adv. Mater.* **2010**, *22*, 3225.
[11] I. Heller, S. Chatoor, J. Mannik, M. A. G. Zevenbergen, C. Dekker, S. G. Lemay, *J. Am. Chem. Soc.* **2010**, *132*, 17149.
[12] a) Q. Wang, X. F. Guo, L. C. Cai, Y. Cao, L. Gan, S. Liu, Z. X. Wang, H. T. Zhang, L. D. Li, *Chem. Sci.* **2011**, *2*, 1860; b) D. Y. Zhang, L. Gan, Y. Cao, Q. Wang, L. M. Qi, X. F. Guo, *Adv. Mater.* **2012**, *24*, 2715; c) M. Kim, N. S. Safron, C. H. Huang, M. S. Arnold, P. Gopalan, *Nano Lett.* **2012**, *12*, 182.
[13] G. Konstantatos, M. Badioli, L. Gaudreau, J. Osmond, M. Bernechea, F. P. G. de Arquer, F. Gatti, F. H. L. Koppens, *Nat. Nanotechnol.* **2012**, *7*, 363.
[14] S. K. Min, W. Y. Kim, Y. Cho, K. S. Kim, *Nat. Nanotechnol.* **2011**, *6*, 162.
[15] S. Stankovich, D. A. Dikin, G. H. B. Dommett, K. M. Kohlhaas, E. J. Zimney, E. A. Stach, R. D. Piner, S. T. Nguyen, R. S. Ruoff, *Nature* **2006**, *442*, 282.
[16] A. Dimiev, D. V. Kosynkin, A. Sinitskii, A. Slesarev, Z. Z. Sun, J. M. Tour, *Science* **2011**, *331*, 1168.
[17] a) J. F. Stoddart, *Chem. Soc. Rev.* **2009**, *38*, 1802; b) B. Champin, P. Mobian, J.-P. Sauvage, *Chem. Soc. Rev.* **2007**, *36*, 358; c) J. D. Crowley, S. M. Goldup, A. L. Lee, D. A. Leigh, R. T. McBurney, *Chem. Soc. Rev.* **2009**, *38*, 1530; d) Y. L. Zhao, J. F. Stoddart, *Acc. Chem. Res.* **2009**, *42*, 1161; e) S. Liu, Q. Shen, Y. Cao, L. Gan, Z. X. Wang, M. L. Steigerwald, X. F. Guo, *Coord. Chem. Rev.* **2010**, *254*, 1101; f) Z. X. Li, J. C. Barnes, A. Bosoy, J. F. Stoddart, J. I. Zink, *Chem. Soc. Rev.* **2012**, *41*, 2590; g) W. R. Browne, B. L. Feringa, *Nat. Nanotechnol.* **2006**, *1*, 25; h) J. E. Green, J. W. Choi, A. Boukai, Y. Bunimovich, E. Johnston-Halperin, E. DeIonno, Y. Luo, B. A. Sheriff, K. Xu, Y. S. Shin, H. R. Tseng, J. F. Stoddart, J. R. Heath, *Nature* **2007**, *445*, 414.
[18] H. Li, A. C. Fahrenbach, A. Coskun, Z. X. Zhu, G. Barin, Y. L. Zhao, Y. Y. Botros, J. P. Sauvage, J. F. Stoddart, *Angew. Chem. Int. Ed.* **2011**, *50*, 6782.
[19] H. T. Zhang, X. F. Guo, J. S. Hui, S. X. Hu, W. Xu, D. B. Zhu, *Nano Lett.* **2011**, *11*, 4939.
[20] Q. A. Shen, L. J. Wang, S. Liu, Y. Cao, L. Gan, X. F. Guo, M. L. Steigerwald, Z. G. Shuai, Z. F. Liu, C. Nuckolls, *Adv. Mater.* **2010**, *22*, 3282.
[21] A. C. Ferrari, J. C. Meyer, V. Scardaci, C. Casiraghi, M. Lazzeri, F. Mauri, S. Piscanec, D. Jiang, K. S. Novoselov, S. Roth, A. K. Geim, *Phys. Rev. Lett.* **2006**, *97*, 187401.
[22] a) R. J. Chen, Y. G. Zhang, D. W. Wang, H. J. Dai, *J. Am. Chem. Soc.* **2001**, *123*, 3838; b) X. F. Guo, L. M. Huang, S. O'Brien, P. Kim, C. Nuckolls, *J. Am. Chem. Soc.* **2005**, *127*, 15045.
[23] a) S. Liu, X. Y. Zhang, W. X. Luo, Z. X. Wang, X. F. Guo, M. L. Steigerwald, X. H. Fang, *Angew. Chem. Int. Ed.* **2011**, *50*, 2496;

b) A. K. M. Newaz, D. A. Markov, D. Prasai, K. I. Bolotin, *Nano Lett.* **2012**, *12*, 2931.

[24] a) E. J. H. Lee, K. Balasubramanian, R. T. Weitz, M. Burghard, K. Kern, *Nat. Nanotechnol.* **2008**, *3*, 486; b) T. Mueller, F. N. A. Xia, P. Avouris, *Nat. Photonics* **2010**, *4*, 297.

[25] N. M. Gabor, J. C. W. Song, Q. Ma, N. L. Nair, T. Taychatanapat, K. Watanabe, T. Taniguchi, L. S. Levitov, P. Jarillo-Herrero, *Science* **2011**, *334*, 648.

[26] M. C. Lemme, F. H. L. Koppens, A. L. Falk, M. S. Rudner, H. Park, L. S. Levitov, C. M. Marcus, *Nano Lett.* **2011**, *11*, 4134.

[27] S. Liu, X. F. Guo, *NPG Asia Mater.* **2012**, *4*, e23.

[28] H. J. Shin, W. M. Choi, D. Choi, G. H. Han, S. M. Yoon, H. K. Park, S. W. Kim, Y. W. Jin, S. Y. Lee, J. M. Kim, J. Y. Choi, Y. H. Lee, *J. Am. Chem. Soc.* **2010**, *132*, 15603.

[29] The AFM image of [2]rotaxane-decorated graphenes shows that the height of tightly-packed SAMs is 7.1 nm, which is similar to the molecular length of **R•**8PF6 (7.4 nm). This result demonstrates that the molecules in the SAMs of **R•**8PF6 stand nearly perpendicularly on the graphene surface. The average coverage of [2]rotaxanes on the graphene surface is estimated to be ≈1 molecules per nm^2.

[30] K. S. Novoselov, A. K. Geim, S. V. Morozov, D. Jiang, Y. Zhang, S. V. Dubonos, I. V. Grigorieva, A. A. Firsov, *Science* **2004**, *306*, 666.

[31] F. Chen, Q. Qing, J. L. Xia, J. H. Li, N. J. Tao, *J. Am. Chem. Soc.* **2009**, *131*, 9908.

[32] A.P. de Silva, *Molecular Logic-Based Computation*, Royal Society of Chemistry, Cambridge, UK **2012**.

[33] F. M. Raymo, S. Giordani, *Encyclopedia of Nanoscience and Nanotechnology, Vol. 5*, (Ed.: H. S. Nalwa), American Scientific Publishers, San Diego, CA, USA **2004**, p. 677.

[34] A. Credi, *Nat. Nanotechnol.* **2008**, *3*, 529.